
Response Uncertainty and Probe Modeling: Two Sides of the Same Coin in LLM Interpretability?

Yongjie Wang, Yibo Wang, Xin Zhou, Zhiqi Shen
Nanyang Technological University, Singapore
{yongjie.wang, xin.zhou, zqshen}@ntu.edu.sg
yibo003@e.ntu.edu.sg

Abstract

Probing techniques have shown promise in revealing how LLMs encode human-interpretable concepts, particularly when applied to curated datasets. However, the factors governing a dataset’s suitability for effective probe training are not well-understood. This study hypothesizes that probe performance on such datasets reflects characteristics of both the LLM’s generated responses and its internal feature space. Through quantitative analysis of probe performance and LLM response uncertainty across a series of tasks, we find a strong correlation: improved probe performance consistently corresponds to a reduction in response uncertainty, and vice versa. Subsequently, we delve deeper into this correlation through the lens of feature importance analysis. Our findings indicate that high LLM response variance is associated with a larger set of important features, which poses a greater challenge for probe models and often results in diminished performance. Moreover, leveraging the insights from response uncertainty analysis, we are able to identify concrete examples where LLM representations align with human knowledge across diverse domains, offering additional evidence of interpretable reasoning in LLMs.

1 Introduction

Large Language Models (LLMs) have demonstrated remarkable performance across a wide range of tasks, including question answering [17], behavioral agency [38, 46], and clinical assistance [40, 44]. Despite these impressive capabilities, some fundamental questions persist: how next-token prediction training yields such broad and functionally useful behaviors, and more specifically, whether LLMs develop a genuine understanding of the physical world [21, 19], or merely capture superficial statistical correlations [10]. To understand LLM internal mechanism, researchers propose various explanatory approaches [42, 41] for enhancing model trustworthiness, particularly in high-stakes applications like healthcare [40, 44] or legal decision-making [14, 15]. Among these, probing-based techniques are widely employed.

Probing-based explanations [6, 26, 9, 21, 34] aim to train a simple auxiliary model (known as probe) that predicts concept attributes (e.g., syntax, toxicity) from representations of a frozen model, thereby elucidating how concepts are encoded within its latent space. Specifically, Testing with Concept Activation Vectors (TCAV) [26] provides quantitative evidence that CNN models capture human-interpretable concepts (e.g., striped patterns). Recent studies [39, 2] demonstrate that LLM representations exhibit significant alignment with human perceptual and conceptual systems in color and spatial domains. Nanda et al. [37] demonstrate that OthelloGPT [30] learns representations of board turn-taking states that could be probed linearly. Gurnee and Tegmark [21] reveal that LLMs encode temporal and spatial representations across multiple scales, whereas Engels et al. [19] show non-linear embedding structures for cyclical temporal concepts (e.g., months/years), challenging the linear representation hypothesis posited by [33].

Building on the success of probing in extracting encoded concepts from LLM internal representations, and recognizing that LLM responses also originate from these representations, we hypothesize that a relationship exists between LLM responses and probing efficacy. Validating this hypothesis serves to bridge the gap between two previously isolated fields: LLM probing and response uncertainty. This connection holds significant practical implications; for instance, it could streamline the identification of LLM-encoded concepts by mitigating the need for laborious data selection and annotation, as well as trial-and-error processes in conventional probing methods.

To verify the aforementioned hypothesis, we conduct extensive experiments investigating the interplay between probe performance and the uncertainty observed in LLM generative responses. Specifically, for each sample in a dataset (e.g., historical figure) in [21], we query the LLM multiple times with an identical prompt (e.g., “Please return the death year of George Washington”) to collect a set of responses. We then compute the response uncertainty for each sample and sort all samples in descending order of this uncertainty. Subsequently, we partition the sorted dataset into several bins and train a separate probe model for each. Finally, we report the correlation between the average response uncertainty and probe performance across these bins. Our results indicate a strong correlation: when an LLM exhibits lower response uncertainty (i.e., less variability in its outputs), its corresponding internal representations can be more accurately modeled by a linear probe.

Moreover, we delve deeper into this observed phenomenon through the lens of feature attribution. Specifically, we adopt AttnLRP (Attention-aware layer-wise relevance propagation) [3], an adaptation of the LRP framework [8] for transformer models, to analyze which features contribute most significantly to the LLM’s response. For latent representations at a specific LLM layer, our experiments reveal that responses with higher uncertainty tend to distribute relevance across a larger number of features compared to those with lower uncertainty, where relevance is more concentrated. This broader distribution of important features poses a significant obstacle for downstream probe models attempting to achieve a good fit, as supported by our theoretical analysis. From our analysis, we establish a clear link between response uncertainty and probe performance, which appear to be two sides of the same coin reflecting the nature of the LLM’s internal representations. Additionally, informed by these findings, we identify specific instances—such as hours, birth years of historical figures, and brand names—where the LLM representations exhibit strong consistency, aligning with human domain knowledge.

Our key contributions are summarized as follows:

- We conducted extensive experiments on six time and space datasets across six public LLMs, demonstrating a strong correlation between LLM response uncertainty and probe performance.
- We provide a mechanistic explanation for this correlation using feature attribution, demonstrating that increased response uncertainty leads to relevance signals distributed across a greater number of features, thus hindering probe model performance. This empirical finding is further supported by our theoretical analysis.
- Our analysis of uncertainty patterns enables the identification of examples where LLM embeddings exhibit significantly consistent with human domain knowledge, yielding more interpretable insights into the model’s internal representations.

2 Preliminaries

Response uncertainty: LLMs often suffer from hallucination issues [32, 23], producing non-factual or fabricated responses that deviate from grounded knowledge. A key observation is that the model’s confidence typically aligns with the correctness and consistency of its outputs, while low-confidence responses (high uncertainty) are more likely to be arbitrary or hallucinatory. Leveraging this insight, response uncertainty has emerged as a valuable signal for detecting potential hallucinations. This uncertainty is commonly quantified by analyzing the variation across multiple response trials and measuring their semantic dispersion using metrics such as response log-likelihood [25], semantic entropy [20, 29, 28], and other methods [16, 24, 48].

LLM probing: Let an LLM f decompose into two modules $f = \varphi \circ \phi$, where ϕ maps a textual input x to a latent representation $\phi(x) \in \mathbb{R}^d$, and φ maps this latent representation $\phi(x)$ to the final generation $\varphi(\phi(x))$. A probing method [6, 9, 53] aims to train a simple probe that predicts the presence or strength of a concept from the LLM latent representation $\phi(x)$. To formally define the

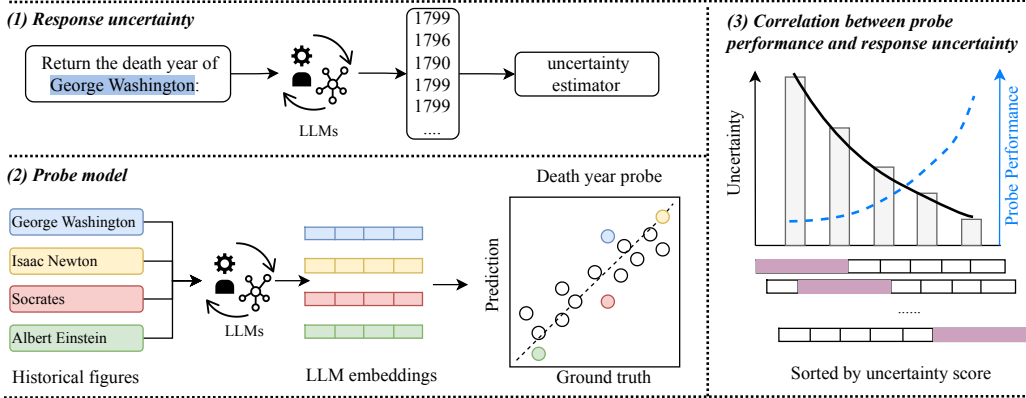


Figure 1: Framework for correlating probe performance with response uncertainty.

probing setup, we consider training a probe model g_θ , parameterized by θ , to predict a target variable Y from LLM representations \mathcal{D} . Here, $\mathcal{D} \in \mathbb{R}^{n \times d}$ represents the latent features for n samples, and Y indicates the presence or strength of a concept, taking either discrete [26, 6, 37] or continuous [21] values. The probe is trained by minimizing a loss function with respect to its parameters θ :

$$L(\theta) = \frac{1}{n} \sum_{i=1}^n \ell(y_i, g_\theta(D_i)) + \lambda \|\theta\|_2^2, \quad (1)$$

where $\ell(\cdot)$ is a loss function (e.g., cross entropy or mean square error) measuring the difference between the probe’s prediction for the i -th sample and its ground truth y_i . High probe performance indicates that the LLM more effectively encodes information relevant to the target concept.

Although extensive studies have investigated either probing approaches or response uncertainty, these research areas are typically studied in isolation. A critical gap persists in understanding the relationship between how well an LLM’s internal representations can be probed for a concept (probe performance) and the uncertainty associated with its generated responses related to that concept. Elucidating this relationship is crucial: it could provide novel insights for diagnosing LLM hallucinations and enable more efficient probing strategies by indicating when the model is unlikely to have effectively encoded the target concept, thereby reducing the need for unnecessary data labeling.

Our idea is motivated by failure cases encountered when probing LLM embeddings for predicting product prices in the Amazon Fashion dataset [22]. In this task, the probe model was unable to learn any meaningful pattern from the LLM’s embeddings, indicating low probe performance. Concurrently, when we directly queried GPT-4 for product prices, it produced highly inconsistent answers, suggesting high response uncertainty. This contrasts sharply with tasks known to be easily probeable [19], where GPT-4 reliably provides correct answers. These observations lead us to hypothesize that *there exists a correlation between LLM response uncertainty and probe performance*.

3 The interplay between probe performance and response uncertainty

3.1 Methodology

To verify our hypothesis, we conducted experiments on six datasets from [21], spanning the domains of history, arts, news, and geography—each involving either time or space concept. For each sample in the dataset, the entity name and additional attributes—such as associated locations, death year, and release date—are recorded. For example, in the historical figures dataset, a sample such as “George Washington” includes attributes like birth year, death year, and other demographic information. Gurnee and Tegmark [21] train a separate regression probe to predict the temporal or space concept from the LLM embedding. More detailed description of six datasets is introduced in Appendix section A.

The workflow of our method is demonstrated in Figure 1. First, for each sample in these datasets, we query an instruction-tuned LLM multiple times (typically 20) with the same prompt to predict

the target concept—for example, “Return the death year of George Washington.” Since LLMs could generate varying responses—such as “1799” or “1796”—we use uncertainty measures to estimate the variability in response behavior. Unlike popular approaches that use entropy to measure uncertainty over discrete predictions [20, 29, 28], our target concept are continuous values. This necessitates using variance as our default metric for response uncertainty [13]. Additionally, we also conduct experiment with entropy as an uncertainty estimator on temporal concepts.

Instead of training a single probe over entire samples for each dataset [21], we sort all samples in decreasing order of response uncertainty. We then divide the sorted dataset into several segments using a sliding window strategy, allowing overlap between consecutive segments. For each segment, we first report the average response uncertainty over all samples within it, and then train a separate probe to assess its performance. Finally, we report the correlation coefficient (e.g., *Kendall and Spearman rank correlation*) between probe performance and average response uncertainty across multiple segments, as shown in Figure 1.

For each segment of samples, we follow the methodology of Gurnee and Tegmark [21] to train the probe model. In particular, each data sample is fed into the same instruction-tuned LLM, and the hidden activations of a target layer are extracted as the data representation. We use the representation of the last token as the sample’s overall representation, following Gurnee and Tegmark [21]. Given a segment with n samples, we obtain a representation dataset $\{D_l, Y\}$ for a target layer l , where Y contains the ground truth of each sample—such as the death year, location, and D_l is the representation set. We split the segment into training and testing sets, and train a linear regression model $\hat{Y} = D_l W$ by optimizing the following objective over the training set,

$$\hat{W} = \arg \min_W \|Y - D_l W\|_2^2 + \lambda \|W\|_2^2, \quad (2)$$

where λ is the regularization term. We report standard regression metrics, including both the R^2 score and the *Spearman rank correlation* on the test set, to evaluate probe performance of each segment. To stabilize probe performance, we randomly split each segment five times using different random seeds and report the average performance across the five trials.

3.2 Implementation details

All of our experiments are conducted on a series of instruction-tuned LLMs, ranging from 8 billion to 72 billion parameters, spanning multiple LLM families including Llama-3.1 (8B, 70B), Qwen 2.5 (14B, 72B) [50], Mistral-Small (24B), and Gemma-2 (27B) [43] series. As reported by Gurnee and Tegmark [21], probe performance typically plateaus after the middle layers of LLMs, and our reproduced probe experiments also support this conclusion. By default, we use the activations of last token from the deeper layer (after the residual connection) as the sample representation. Since probe performance stabilizes after the middle layers, the choice of target layer does not affect our conclusions as long as it is no shallower than the middle layer.

For larger LLMs with higher-dimensional representations, we use a larger window size that contains more samples to mitigate overfitting. Additional details are provided in Appendix B, including the window size and stride used for segment division, probe training configurations, and the target layer selected for each LLM.

4 Experiment results

4.1 Existence of high correlation

In this experiment, we investigate the correlation between LLM response uncertainty and probe performance across six datasets using six public LLMs. As shown in Figure 2, probe performance generally increases with decreased response uncertainty. Despite minor fluctuations, a strong negative correlation is observed. We report the correlation scores in Table 1, where both Kendall and Spearman rank correlation coefficients typically fall below -0.5 , often approaching -1 , indicating a strong negative correlation between these two factors. Exceptions include the USA dataset for larger models such as Llama 3.1 70B and Qwen 2.5 72B, where the LLMs produce highly consistent responses across most samples, making it difficult to validate our hypothesis. Similarly, on the World dataset, LLMs exhibit very low response uncertainty for many samples, thus, we report the correlation using only the top 20,000 most uncertain samples.

Table 1: Correlation coefficients between probe performance and LLM response uncertainty on Llama 3.1 (8B, 70B), Qwen 2.5 (14B, 72B), Mistral-Small (24B), and Gemma-2 (27B). Symbol ‘—’ indicates uniformly low uncertainty over almost all samples; underscored values are computed on the top 20,000 most uncertain samples.

Dataset	LLama 8B		LLama 70B		Qwen 14B		Qwen 72B		Mistral 24B		Gemma 27B	
	K	Sp										
<i>Correlation coefficient: response uncertainty (variance) vs probe performance (R^2).</i>												
Figures	-0.89	-0.98	-0.76	-0.88	-0.71	-0.83	-0.79	-0.92	-0.86	-0.95	-0.96	-0.99
Artworks	-0.94	-0.99	-0.97	-0.93	-0.81	-0.93	-0.79	-0.94	-0.90	-0.97	-0.89	-0.97
News	-0.57	-0.71	-0.92	-0.98	-0.45	-0.67	-0.41	-0.68	-0.78	-0.90	-0.93	-0.99
NYC	-0.89	-0.96	-0.80	-0.90	-0.88	-0.96	-0.96	-0.99	-0.97	-0.99	-0.75	-0.88
USA	-0.91	-0.98	—	—	-0.86	-0.94	—	—	-0.72	-0.87	-0.91	-0.96
World	<u>-0.80</u>	<u>-0.92</u>	<u>-0.89</u>	<u>-0.91</u>	<u>-0.69</u>	<u>-0.74</u>	<u>-0.89</u>	<u>-0.97</u>	<u>-0.92</u>	<u>-0.98</u>	<u>-0.96</u>	<u>-0.99</u>
<i>Correlation coefficient: response uncertainty (variance) vs probe performance (Spearman rank correlation).</i>												
Figures	-0.67	-0.82	-0.77	-0.90	-0.82	-0.95	-0.55	-0.72	-0.86	-0.96	-0.89	-0.97
Artworks	-0.96	-0.99	-0.94	-0.87	-0.77	-0.91	-0.79	-0.93	-0.90	-0.97	-0.88	-0.97
News	-0.57	-0.72	-0.93	-0.99	-0.45	-0.66	-0.68	-0.85	-0.82	-0.93	-0.92	-0.98
NYC	-0.85	-0.91	-0.80	-0.90	-0.93	-0.97	-1.00	-1.00	-0.95	-0.99	-0.86	-0.94
USA	-0.87	-0.96	—	—	-0.88	-0.91	—	—	-0.71	-0.85	-0.74	-0.89
World	<u>-0.84</u>	<u>-0.93</u>	<u>-0.89</u>	<u>-0.92</u>	<u>-0.77</u>	<u>-0.86</u>	<u>-0.83</u>	<u>-0.78</u>	<u>-0.89</u>	<u>-0.97</u>	<u>-0.86</u>	<u>-0.95</u>

- ‘K’ and ‘Sp’ denote the Kendall and Spearman rank correlation coefficients respectively.

When response uncertainty is measured with entropy on the first three temporal datasets, the same conclusion still holds, as shown in the Appendix section C. (Note that entropy is not suited for location predictions, such as latitude and longitude, where even small numerical differences can correspond to large spatial differences on the map.) One interesting question is whether the correlation is linear. In our experiment (Appendix section D), we find that linearity depends on the choice of uncertainty estimator. Since entropy and variance operate on different scales depending on the numerical range of the ground truth, their behavior varies. When using entropy as the uncertainty measure, the Pearson correlation is strongly negative, whereas it is relatively low when using variance. We leave a deeper investigation into the conditions under which linearity holds in general cases to future work.

4.2 Sensitivity experiments

To assess the robustness of our findings with respect to key parameters—such as generation temperatures, the sliding window strategy for the probe model, and prompt selection—we conducted a series of sensitivity experiments, as presented below.

Generation temperature. Temperature controls the creativity and randomness of LLM responses: lower values typically result in more deterministic outputs, while higher values lead to more varied and stochastic responses. In this experiment, we regenerate responses using different temperatures, ranging from 0.1 to 1.5. We then report the correlation coefficients under each temperature setting, as shown in the Figure 3. The results show that the correlation remains relatively stable across the temperature range of [0.1, 1], which covers the standard default range for most LLMs.

Sliding window strategy. The window and stride control how many samples are included in each segment and determine the total number of segments. Too few samples per segment can lead to unstable probe training, while too few segments may render the correlation estimates unreliable. In this experiment, we plot the Spearman correlation scores between response uncertainty (variance) and probe performance (Spearman rank coefficients) under different window and stride settings in Figure 4 on the *Figures* dataset. Despite slight variations in the coefficient values, our main findings are not sensitive to this selection, as long as the two factors are not set to extreme values.

Prompt. Different prompts inevitably affect the quality of generated responses, especially when advanced prompting strategies such as chain-of-thought reasoning or in-context examples are employed. In this study, we experiment with various simple prompts while keeping the core objective fixed: querying LLMs to answer a specific target concept. These variations include instructions such as asking the model to “play as a historian” or adding restriction for output format to guide the response.

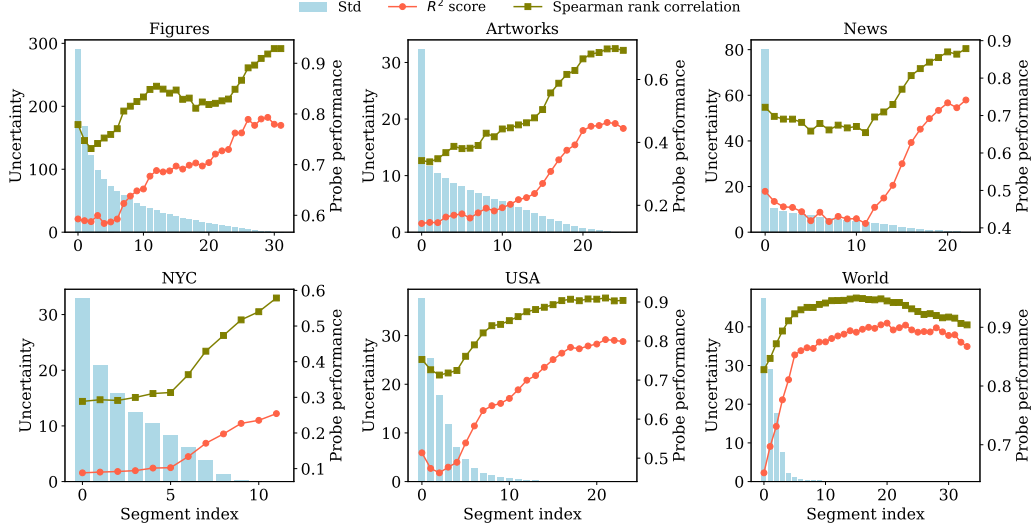


Figure 2: Trend between response uncertainty and probe performance on the Llama 3.1 (8B) model over all six datasets.

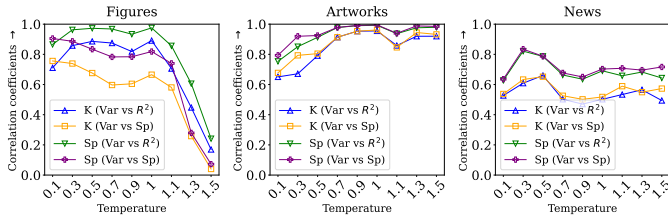


Figure 3: The correlation analysis with different temperatures in generation for Llama 3.1 (8B). ‘Var’, ‘K’, and ‘Sp’ denotes variance (uncertainty estimator), Kendall and Spearman rank correlation coefficients. Here, we use absolute value for good visualization.

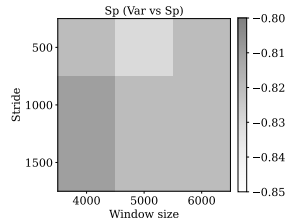


Figure 4: Correlation coefficient vs sliding window parameters, Llama 3.1 (8B) on Figures.

The prompt templates and results, shown in Table 6 of Appendix E, indicate that the correlation persists regardless of the slight difference in prompt template.

5 Exploring the mechanisms underlying the correlation

In this study, we analyze the correlation between response uncertainty and probe performance from a causal perspective, targeting to identify a confounding factor that could influence both. We hypothesize that *the target concept is encoded in a set of features within the LLM embeddings that are shared by both the probe model and the generation process.*

To investigate this, we first examine the importance scores of latent representation $\phi(x) \in \mathbb{R}^d$ with respect to an LLM’s response, using AttnLRP [3, 7]. This yields a feature importance vector $\sigma(x) \in \mathbb{R}^d$, where each value reflects the contribution of the corresponding feature of $\phi(x)$ to the that response. A higher importance score indicates that removing the corresponding feature would result in a significant degradation in response quality. *If both the probe model and the LLM generation rely on the same set of features, we would expect the probe model to preserve similar predictions when using the important features of response generation, compared to the original full representation.*

After obtaining the feature importance vector by tracing back from the response, we gradually mask the unimportant features by zeroing them out and observe the performance drop in the probe model. We evaluate the degradation from two perspectives: (i) freezing the probe weights and directly test the probe performance on masked representations [47]. Note this probe model is trained on the entire dataset; and (ii) masking the important features across all samples, retraining the probe model,

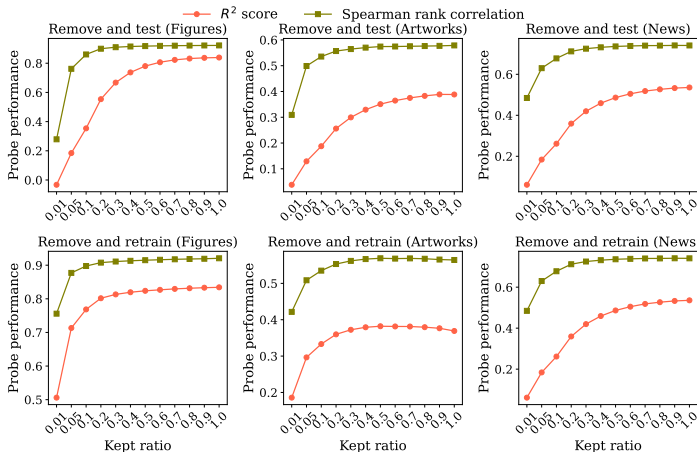


Figure 5: Llama 3.1 (8B) model. We gradually remove unimportant features to LLM responses and observe the probe performance drop.

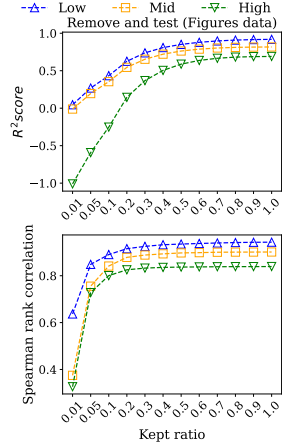


Figure 6: Remove and test on differently uncertain subsets, Llama 3.1 (8B).

and reporting its performance on the masked test set—following the Remove and Retrain (RoAR) paradigm [4].

The results are reported in Figure 5, where the x -axis represents the ratio of important features preserved (with the remaining features zeroed out), and the y -axis indicates the performance of the probe model. From them, we observe that even when only a small fraction of the most important features for the LLM response is preserved, the probe model can achieve performance comparable to using the full set of features. For example, preserving the top-30% important features could achieve the similar results with the entire features on the Figure dataset in term of R^2 score. In the remove-and-retraining experiments, keeping top-20% important features could achieve a good fit for probe models. These experiments provide strong evidence supporting the observed correlation: *both the LLM and the probe model rely on the similar set of features relevant to the target concept.*

5.1 Higher uncertainty implies more important features

In this section, we present both theoretical and empirical analyses to investigate *why response uncertainty is negatively correlated with probe performance across subsets with varying levels of uncertainty.*

Mathematical analysis: Suppose the set of important features for a given response r_i is denoted as $\hat{\phi}_i(x) \in \mathbb{R}^k \subseteq \phi(x)$, where $k \ll d$, following the sparse representation findings of [31, 45]. If an LLM exhibits higher variation in its response to the same question, different responses are likely to track back to different important features in $\phi(x)$. This suggests that a larger number of features (i.e., the union of $\hat{\phi}_i(x)$) should be deemed important, resulting in a more broadly distributed importance scores. According to the Lasso oracle inequality in compressed sensing domain [11], the generalization bound of ridge regression is proportional to the ratio of important feature used with a constant probability. This implies that the probe is likely to perform worse when more features contribute significantly to the prediction, as it becomes harder to learn a stable and low-dimensional mapping. The detailed mathematical analysis is provided in the Appendix section G.

To verify this, we construct three subsets of 5,000 samples, selected based on varying levels of response uncertainty, referred to as Low, Mid, and High for brevity. We train a probe model for the entire dataset and observe the performance drop for each subset as unimportant features are progressively masked. The experimental results on the Figures dataset using Llama 3.1 (8B) are shown in Figure 6. We can clearly see that the probe trained on the high-uncertainty subset requires a larger number of features to maintain comparable performance, whereas the probe trained on the low-uncertainty subset achieves similar performance using relatively fewer features. For example, preserving the top 40% of important features approximately restores the probe performance for the high-uncertainty subset, while retaining only the top 20% is sufficient for the low-uncertainty subset,

as shown in the upper figure. In the bottom figure, preserving the top 5% of important features is sufficient to achieve a similar Spearman score for the probe performance on the low-uncertainty subset, whereas 10% is needed for the high-certainty subset. Due to page limit, we put more experiments that support this conclusion in the Appendix section F.

5.2 Probe examples guided by response uncertainty

Guided by our hypothesis, we identified several examples in which LLM embeddings encode human-interpretable knowledge that can be effectively visualized or extracted using a probing model, shown in Figure 7. In these cases, LLM also produces highly consistent responses to questions like “What is the category of {}” and “What hour is after {}?”, as shown in Table 7 (Appendix). We extract the embedding of each entity name from layer 25 of Llama 3.1 (8B). For the first two examples, we project the embeddings into two dimensions using T-SNE. For the third example, we train a linear probe to predict the birth year from the same embeddings.

As shown in Figure 7, the left panel visualizes embeddings of common brands such as Nike, Adidas, and Armani. We observe that luxury brands (e.g., LV, Burberry) cluster together, while sports brands (e.g., Nike, Adidas, Puma) form a separate cluster—indicating that the LLM captures categorical distinctions among brand types. The middle panel shows temporal representations from 0 a.m. to 11 p.m., revealing a circular pattern in the embedding space that aligns with typical daily activity cycles. In the right figure, we apply the linear regression probe to predict birth year from the embeddings of historical figures’ names. We see that our probe achieve good fit compared to the results for death year prediction reported in [21]. This example shows that the embedding of a figure’s name encodes rich information, which can be effectively extracted using different probing methods.

From the above three examples, we also observe that for mono-semantic entities, the embedding visualization often aligns well with human prior knowledge. In contrast, for entities with stereo-semantic meanings, a probe model is required to extract a specific target concept.

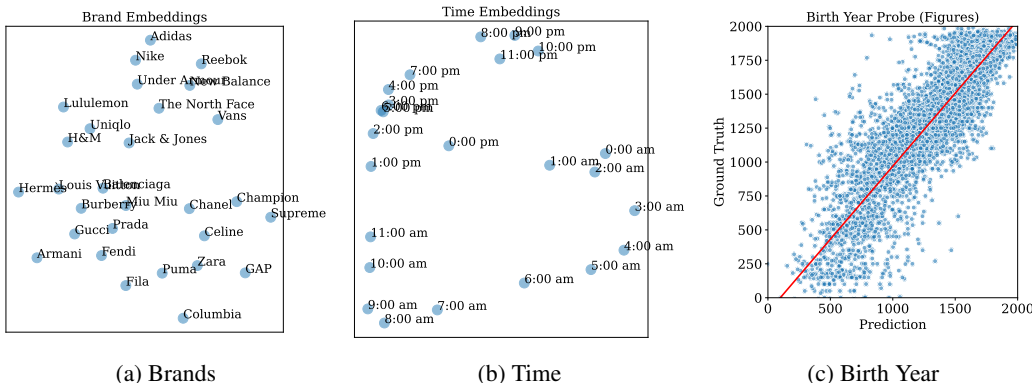


Figure 7: Three commonsense examples where LLM embeddings align well with human knowledge or are easily probed, identified through consistent LLM responses.

6 Related work

LLM interpretability. The lack of interpretability limits the deployment of LLMs in high-stakes applications. To address this challenge, a range of approaches has been proposed to explain and interpret the behaviors and predictions of LLMs [53, 42, 47]. These methods include assessing the importance of input tokens in next-token prediction [3, 7], analyzing transformer circuits [18, 36], and elucidating the reasoning processes behind LLM outputs [49, 51].

Our study falls within the scope of probe-based explanation methods, which aim to interpret LLMs at a global level. A probe—typically a simple, trained model—is utilized to detect the presence of a target concept from the embeddings produced by the LLM, usually adhering to the linear representation hypothesis [33]. Generally, probe models are trained on external datasets containing training instances of the target concepts (e.g., low-level stripes in TCAV [26], color attributes [39], or

spatial and temporal concepts [21], game status [30]). Some other works propose to automatically learn concepts during CNN training without relying on external probe datasets [27, 52, 12]. A recent study provides strong evidence supporting circular representations for temporal concepts such as ‘week’ and ‘year,’ thus challenging the traditional linear hypothesis [33]. However, to the best of our knowledge, no prior work has comprehensively investigated the relationship between probe performance and generative behavior in LLMs.

LLM hallucination. LLMs often generate non-factual or fabricated responses that deviate from grounded knowledge, stemming from various factors such as insufficient coverage in the training data or limited model capacity. For uncertainty that arises when the ground truth is deterministic—referred to as epistemic uncertainty [1]—researchers commonly use uncertainty measures to quantify the dispersion across multiple responses. Most studies [25, 20, 29, 28] focus on developing metrics to more accurately measure response uncertainty from different perspectives, while largely overlooking the implications of these measurements.

7 Limitations and discussion

Although our extensive experiments demonstrate a strong correlation between probe performance and response uncertainty, several interesting phenomena remain poorly understood. We discuss these observations below and also highlight open questions for future work.

Probe weights and prompt embeddings. A growing body of evidence shows that LLM hidden representations encode conceptual information that can be effectively extracted using probing models. Simultaneously, such information can also be elicited through carefully designed prompts. We hypothesize that prompts function in a manner analogous to probes, although the mechanism remains poorly understood. In future work, it would be valuable to gather concrete evidence to test this hypothesis.

What happened during instruction tuning. In our experiments, a stronger correspondence between probe performance and response consistency is observed only in instruction-tuned models. In contrast, for base LLMs, even when the probe achieves a good fit, the generated responses often remain disorganized and fail to answer questions accurately. This observation motivates further investigation into the parameter changes introduced by instruction tuning [35], particularly in the later layers of the model.

Concept encoding and decoding process. Our case study demonstrates that LLMs encode rich information—for example, both birth and death years, within the representation of a person’s name—which can be extracted using different probes. Similar conclusions have been drawn by Adly et al. [5]. We are particularly interested in understanding how such information is encoded and the internal mechanisms that govern its decoding, whether through probing models or user prompts.

A unified interpretability framework. In this paper, we present strong evidence between these response uncertainty and LLM probe, suggesting that either method could be used to evaluate LLMs depending on practical availability. For example, response uncertainty may serve as a lightweight diagnostic tool when probing is not feasible. Alternatively, we could investigate whether a probe model applied to latent representations can be used to estimate response uncertainty [28]. More importantly, it is worth investigating whether similar correlations exist across other interpretability methods, with the long-term goal of developing a unified framework for LLM explanation.

8 Conclusion

In this paper, we demonstrated a strong correlation between LLM response uncertainty and probe performance. Specifically, when the probe achieves higher performance, the LLM tends to produce more consistent responses, and vice versa. Furthermore, we delve deeper into this correlation from the feature importance analysis. Our findings reveal that high response uncertainty is typically associated with a larger number of important features, making it more challenging to effectively train a probing model. Finally, we identified concrete examples characterized by low response uncertainty, where the representation visualizations closely align with human knowledge or can be easily probed.

References

- [1] Yasin Abbasi Yadkori, Ilja Kuzborskij, András György, and Csaba Szepesvari. To believe or not to believe your llm: Iterative prompting for estimating epistemic uncertainty. *Advances in Neural Information Processing Systems*, 37:58077–58117, 2024.
- [2] Mostafa Abdou, Artur Kulmizev, Daniel Hershcovich, Stella Frank, Ellie Pavlick, and Anders Søgaard. Can language models encode perceptual structure without grounding? a case study in color. In *Proceedings of the 25th Conference on Computational Natural Language Learning*, pages 109–132, 2021.
- [3] Reduan Achtibat, Sayed Mohammad Vakilzadeh Hatefi, Maximilian Dreyer, Aakriti Jain, Thomas Wiegand, Sebastian Lapuschkin, and Wojciech Samek. Attnlrp: attention-aware layer-wise relevance propagation for transformers. In *Proceedings of the 41st International Conference on Machine Learning, ICML’24*. JMLR.org, 2024.
- [4] Julius Adebayo, Justin Gilmer, Michael Muehly, Ian Goodfellow, Moritz Hardt, and Been Kim. Sanity checks for saliency maps. *Advances in neural information processing systems*, 31, 2018.
- [5] Templeton Adly, Conerly Tom, Marcus Jonathan, Lindsey Jack, Bricken Trenton, Chen Brian, et al. Scaling monosemanticity: Extracting interpretable features from claude 3 sonnet. *Transformer Circuits Thread*, 2024.
- [6] Guillaume Alain and Yoshua Bengio. Understanding intermediate layers using linear classifier probes. In *The Fifth International Conference on Learning Representations*, 2017. URL <https://openreview.net/forum?id=ryF7rTqg1>.
- [7] Leila Arras, Bruno Puri, Patrick Kahardipraja, Sebastian Lapuschkin, and Wojciech Samek. A close look at decomposition-based xai-methods for transformer language models. *arXiv preprint arXiv:2502.15886*, 2025.
- [8] Sebastian Bach, Alexander Binder, Grégoire Montavon, Frederick Klauschen, Klaus-Robert Müller, and Wojciech Samek. On pixel-wise explanations for non-linear classifier decisions by layer-wise relevance propagation. *PLoS one*, 10(7):e0130140, 2015.
- [9] Yonatan Belinkov. Probing classifiers: Promises, shortcomings, and advances. *Computational Linguistics*, 48(1):207–219, March 2022. doi: 10.1162/coli_a_00422. URL <https://aclanthology.org/2022.c1-1.7/>.
- [10] Emily M. Bender and Alexander Koller. Climbing towards NLU: On meaning, form, and understanding in the age of data. In Dan Jurafsky, Joyce Chai, Natalie Schluter, and Joel Tetreault, editors, *Proceedings of the 58th Annual Meeting of the Association for Computational Linguistics*, pages 5185–5198, Online, July 2020. Association for Computational Linguistics. doi: 10.18653/v1/2020.acl-main.463. URL <https://aclanthology.org/2020.acl-main.463/>.
- [11] Peter Bühlmann and Sara Van De Geer. *Statistics for high-dimensional data: methods, theory and applications*. Springer Science & Business Media, 2011.
- [12] Collin Burns, Haotian Ye, Dan Klein, and Jacob Steinhardt. Discovering latent knowledge in language models without supervision. In *The Eleventh International Conference on Learning Representations*.
- [13] Christopher Bülte, Yusuf Sale, Timo Löhr, Paul Hofman, Gitta Kutyniok, and Eyke Hüllermeier. An axiomatic assessment of entropy- and variance-based uncertainty quantification in regression, 2025. URL <https://arxiv.org/abs/2504.18433>.
- [14] Inyoung Cheong, King Xia, KJ Kevin Feng, Quan Ze Chen, and Amy X Zhang. (a) i am not a lawyer, but...: engaging legal experts towards responsible llm policies for legal advice. In *Proceedings of the 2024 ACM Conference on Fairness, Accountability, and Transparency*, pages 2454–2469, 2024.

- [15] Pierre Colombo, Telmo Pires, Malik Boudiaf, Rui Filipe Coimbra Pereira de Melo, Gabriel Hautreux, Etienne Malaboeuf, Johanne Charpentier, Dominic Culver, and Michael Desa. SaulLM-54b & saulLM-141b: Scaling up domain adaptation for the legal domain. In *The Thirty-eighth Annual Conference on Neural Information Processing Systems*, 2024. URL <https://openreview.net/forum?id=NLUYZ4ZqNq>.
- [16] Vikranth Dwaracherla, Zheng Wen, Ian Osband, Xiuyuan Lu, Seyed Mohammad Asghari, and Benjamin Van Roy. Ensembles for uncertainty estimation: Benefits of prior functions and bootstrapping. *Transactions on Machine Learning Research*, 2023. ISSN 2835-8856. URL <https://openreview.net/forum?id=IqJsyu1DUX>.
- [17] Darren Edge, Ha Trinh, Newman Cheng, Joshua Bradley, Alex Chao, Apurva Mody, Steven Truitt, Dasha Metropolitanaky, Robert Osazuwa Ness, and Jonathan Larson. From local to global: A graph rag approach to query-focused summarization. *arXiv preprint arXiv:2404.16130*, 2024.
- [18] Nelson Elhage, Neel Nanda, Catherine Olsson, Tom Henighan, Nicholas Joseph, Ben Mann, Amanda Askell, Yuntao Bai, Anna Chen, Tom Conerly, et al. A mathematical framework for transformer circuits. *Transformer Circuits Thread*, 1(1):12, 2021.
- [19] Joshua Engels, Eric J Michaud, Isaac Liao, Wes Gurnee, and Max Tegmark. Not all language model features are one-dimensionally linear. In *The Thirteenth International Conference on Learning Representations*, 2025. URL <https://openreview.net/forum?id=d63a4AM4hb>.
- [20] Sebastian Farquhar, Jannik Kossen, Lorenz Kuhn, and Yarin Gal. Detecting hallucinations in large language models using semantic entropy. *Nature*, 630(8017):625–630, 2024.
- [21] Wes Gurnee and Max Tegmark. Language models represent space and time. In *The Twelfth International Conference on Learning Representations*, 2024. URL <https://openreview.net/forum?id=jE8xbmvFin>.
- [22] Yupeng Hou, Jiacheng Li, Zhankui He, An Yan, Xiushi Chen, and Julian McAuley. Bridging language and items for retrieval and recommendation. *arXiv preprint arXiv:2403.03952*, 2024.
- [23] Ziwei Ji, Nayeon Lee, Rita Frieske, Tiezheng Yu, Dan Su, Yan Xu, Etsuko Ishii, Ye Jin Bang, Andrea Madotto, and Pascale Fung. Survey of hallucination in natural language generation. *ACM Comput. Surv.*, 55(12), March 2023. ISSN 0360-0300. doi: 10.1145/3571730. URL <https://doi.org/10.1145/3571730>.
- [24] Daniel D. Johnson, Daniel Tarlow, David Duvenaud, and Chris J. Maddison. Experts don’t cheat: Learning what you don’t know by predicting pairs. In Ruslan Salakhutdinov, Zico Kolter, Katherine Heller, Adrian Weller, Nuria Oliver, Jonathan Scarlett, and Felix Berkenkamp, editors, *Proceedings of the 41st International Conference on Machine Learning*, volume 235 of *Proceedings of Machine Learning Research*, pages 22406–22464. PMLR, 21–27 Jul 2024. URL <https://proceedings.mlr.press/v235/johnson24a.html>.
- [25] Saurav Kadavath, Tom Conerly, Amanda Askell, Tom Henighan, Dawn Drain, Ethan Perez, Nicholas Schiefer, Zac Hatfield-Dodds, Nova DasSarma, Eli Tran-Johnson, et al. Language models (mostly) know what they know. *arXiv preprint arXiv:2207.05221*, 2022.
- [26] Been Kim, Martin Wattenberg, Justin Gilmer, Carrie Cai, James Wexler, Fernanda Viegas, et al. Interpretability beyond feature attribution: Quantitative testing with concept activation vectors (tcav). In *International conference on machine learning*, pages 2668–2677. PMLR, 2018.
- [27] Pang Wei Koh, Thao Nguyen, Yew Siang Tang, Stephen Mussmann, Emma Pierson, Been Kim, and Percy Liang. Concept bottleneck models. In *International conference on machine learning*, pages 5338–5348. PMLR, 2020.
- [28] Jannik Kossen, Jiatong Han, Muhammed Razzak, Lisa Schut, Shreshth A Malik, and Yarin Gal. Semantic entropy probes: Robust and cheap hallucination detection in LLMs, 2025. URL <https://openreview.net/forum?id=YQvvJjLWX0>.

- [29] Lorenz Kuhn, Yarin Gal, and Sebastian Farquhar. Semantic uncertainty: Linguistic invariances for uncertainty estimation in natural language generation. In *The Eleventh International Conference on Learning Representations*, 2023. URL <https://openreview.net/forum?id=VD-AYtPOdve>.
- [30] Kenneth Li, Aspen K Hopkins, David Bau, Fernanda Viégas, Hanspeter Pfister, and Martin Wattenberg. Emergent world representations: Exploring a sequence model trained on a synthetic task. In *The Eleventh International Conference on Learning Representations*, 2023. URL https://openreview.net/forum?id=DeG07_TcZvT.
- [31] Yuqi Luo, Chenyang Song, Xu Han, Yingfa Chen, Chaojun Xiao, Zhiyuan Liu, and Maosong Sun. Sparsing law: Towards large language models with greater activation sparsity. *arXiv preprint arXiv:2411.02335*, 2024.
- [32] Joshua Maynez, Shashi Narayan, Bernd Bohnet, and Ryan McDonald. On faithfulness and factuality in abstractive summarization. In Dan Jurafsky, Joyce Chai, Natalie Schluter, and Joel Tetreault, editors, *Proceedings of the 58th Annual Meeting of the Association for Computational Linguistics*, pages 1906–1919, Online, July 2020. Association for Computational Linguistics. doi: 10.18653/v1/2020.acl-main.173. URL <https://aclanthology.org/2020.acl-main.173/>.
- [33] Tomas Mikolov, Wen-tau Yih, and Geoffrey Zweig. Linguistic regularities in continuous space word representations. In Lucy Vanderwende, Hal Daumé III, and Katrin Kirchhoff, editors, *Proceedings of the 2013 Conference of the North American Chapter of the Association for Computational Linguistics: Human Language Technologies*, pages 746–751, Atlanta, Georgia, June 2013. Association for Computational Linguistics. URL <https://aclanthology.org/N13-1090/>.
- [34] Tomáš Mikolov, Wen-tau Yih, and Geoffrey Zweig. Linguistic regularities in continuous space word representations. In *Proceedings of the 2013 conference of the north american chapter of the association for computational linguistics: Human language technologies*, pages 746–751, 2013.
- [35] Julian Minder, Clement Dumas, Caden Juang, Bilal Chughtai, and Neel Nanda. Robustly identifying concepts introduced during chat fine-tuning using crosscoders. *arXiv preprint arXiv:2504.02922*, 2025.
- [36] Neel Nanda, Lawrence Chan, Tom Lieberum, Jess Smith, and Jacob Steinhardt. Progress measures for grokking via mechanistic interpretability. In *The Eleventh International Conference on Learning Representations*, 2023. URL <https://openreview.net/forum?id=9XFSbDPmdW>.
- [37] Neel Nanda, Andrew Lee, and Martin Wattenberg. Emergent linear representations in world models of self-supervised sequence models. In Yonatan Belinkov, Sophie Hao, Jaap Jumelet, Najaoung Kim, Arya McCarthy, and Hosein Mohebbi, editors, *Proceedings of the 6th BlackboxNLP Workshop: Analyzing and Interpreting Neural Networks for NLP*, pages 16–30, Singapore, December 2023. Association for Computational Linguistics. doi: 10.18653/v1/2023.blackboxnlp-1.2. URL <https://aclanthology.org/2023.blackboxnlp-1.2/>.
- [38] Joon Sung Park, Joseph O’Brien, Carrie Jun Cai, Meredith Ringel Morris, Percy Liang, and Michael S Bernstein. Generative agents: Interactive simulacra of human behavior. In *Proceedings of the 36th annual acm symposium on user interface software and technology*, pages 1–22, 2023.
- [39] Roma Patel and Ellie Pavlick. Mapping language models to grounded conceptual spaces. In *International Conference on Learning Representations*, 2022. URL <https://openreview.net/forum?id=gJcEM8sxHK>.
- [40] Jianing Qiu, Kyle Lam, Guohao Li, Amish Acharya, Tien Yin Wong, Ara Darzi, Wu Yuan, and Eric J Topol. Llm-based agentic systems in medicine and healthcare. *Nature Machine Intelligence*, 6(12):1418–1420, 2024.

- [41] Pratyusha Sharma, Jordan T. Ash, and Dipendra Misra. The truth is in there: Improving reasoning in language models with layer-selective rank reduction. In *The Twelfth International Conference on Learning Representations*, 2024. URL <https://openreview.net/forum?id=ozX92bu8VA>.
- [42] Chandan Singh, Jeevana Priya Inala, Michel Galley, Rich Caruana, and Jianfeng Gao. Rethinking interpretability in the era of large language models. *arXiv preprint arXiv:2402.01761*, 2024.
- [43] Gemma Team. Gemma 3. 2025. URL <https://goo.gle/Gemma3Report>.
- [44] Arun James Thirunavukarasu, Darren Shu Jeng Ting, Kabilan Elangovan, Laura Gutierrez, Ting Fang Tan, and Daniel Shu Wei Ting. Large language models in medicine. *Nature medicine*, 29(8):1930–1940, 2023.
- [45] Elena Voita, David Talbot, Fedor Moiseev, Rico Sennrich, and Ivan Titov. Analyzing multi-head self-attention: Specialized heads do the heavy lifting, the rest can be pruned. In *Proceedings of the 57th Annual Meeting of the Association for Computational Linguistics*, pages 5797–5808, 2019.
- [46] Guanzhi Wang, Yuqi Xie, Yunfan Jiang, Ajay Mandlekar, Chaowei Xiao, Yuke Zhu, Linxi Fan, and Anima Anandkumar. Voyager: An open-ended embodied agent with large language models. *Transactions on Machine Learning Research*, 2024. ISSN 2835-8856. URL <https://openreview.net/forum?id=ehfRiF0R3a>.
- [47] Yongjie Wang, Tong Zhang, Xu Guo, and Zhiqi Shen. Gradient based feature attribution in explainable ai: A technical review. *arXiv preprint arXiv:2403.10415*, 2024.
- [48] Zi Wang, Alexander Ku, Jason Baldridge, Tom Griffiths, and Been Kim. Gaussian process probes (gpp) for uncertainty-aware probing. *Advances in neural information processing systems*, 36:63573–63594, 2023.
- [49] Jason Wei, Xuezhi Wang, Dale Schuurmans, Maarten Bosma, Fei Xia, Ed Chi, Quoc V Le, Denny Zhou, et al. Chain-of-thought prompting elicits reasoning in large language models. *Advances in neural information processing systems*, 35:24824–24837, 2022.
- [50] An Yang, Baosong Yang, Beichen Zhang, Binyuan Hui, Bo Zheng, Bowen Yu, Chengyuan Li, Dayiheng Liu, Fei Huang, Haoran Wei, et al. Qwen2. 5 technical report. *arXiv preprint arXiv:2412.15115*, 2024.
- [51] Shunyu Yao, Dian Yu, Jeffrey Zhao, Izhak Shafran, Tom Griffiths, Yuan Cao, and Karthik Narasimhan. Tree of thoughts: Deliberate problem solving with large language models. *Advances in neural information processing systems*, 36:11809–11822, 2023.
- [52] Chih-Kuan Yeh, Been Kim, Sercan Arik, Chun-Liang Li, Tomas Pfister, and Pradeep Ravikumar. On completeness-aware concept-based explanations in deep neural networks. *Advances in neural information processing systems*, 33:20554–20565, 2020.
- [53] Haiyan Zhao, Hanjie Chen, Fan Yang, Ninghao Liu, Huiqi Deng, Hengyi Cai, Shuaiqiang Wang, Dawei Yin, and Mengnan Du. Explainability for large language models: A survey. *ACM Trans. Intell. Syst. Technol.*, 15(2), February 2024. ISSN 2157-6904. doi: 10.1145/3639372. URL <https://doi.org/10.1145/3639372>.

A Dataset description

Our experiments are conducted on three spatial and three temporal datasets collected by Gurnee and Tegmark [21]. Each dataset contains the names of entities—such as celebrities, news headlines, artworks, or places—along with their associated spatial and temporal attributes. In [21], the authors propose learning a regression probe to extract spatial or temporal information from entity embeddings. Table 2 summarizes the number of samples in each dataset and provides a representative example. Since we prompt LLMs to generate responses related to specific concepts, we also list the corresponding prompts. Here we use simple prompts only, without employing advanced prompting strategies such as chain-of-thought or in-context examples. By default, the temperature for response generation is set to 1, which is the default setting in the HuggingFace pipeline generator.

Table 2: Descriptions of the datasets and prompts used to generate LLM responses.

Dataset	Count	Example	Prompt Template
Figures	37,539	“Cleopatra”	Return the death year of { }
Artworks	31,321	“Stephen King’s It”	Return the release year of { }
News	28,389	“Dozens Rescued From ... ”	Return the publish year of { }
NYC	19,838	“Borden Avenue Bridge”	Return the latitude and longitude of { } in NYC
USA	29,997	“Columbia University”	Return the latitude and longitude of { } in USA
World	39,585	“Los Angeles”	Return the latitude and longitude of { }

B Additional implementation details

In this section, we provide additional details about our experimental setup. Table 3 summarizes the settings used for training the probe model. Due to the higher feature dimensionality in large LLMs such as Llama 3.1 (70B), a larger number of samples is required. To manage this, we set different window sizes and strides. For each sample, we extract the representation from the 25th layer, using the hidden state of the last token.

During probe training, we randomly split the data—whether a segment, a subset, or the entire dataset depending on the experimental setting—into training and test sets at a 4 : 1 ratio. The training set is further divided into two parts: one for training the probe and the other for tuning the trade-off parameter λ . We report both the R^2 score and the Spearman rank correlation coefficient on the test set.

By default, we use the prompt template shown in Table 2 to generate multiple responses for each sample. We also experiment with alternative prompt formats on the Figures dataset with Llama 3.1 8B model, as listed in Table 6.

Table 3: Target layer, representation dimension and sliding window settings (window size and stride) for different LLMs.

Model	Target layer	#Layers	Dimension	Window size	Stride
Llama 3.1 (8B)	25	32	4096	6000	1000
Llama 3.1 (70B)	60	80	8192	12000	1000
Qwen 2.5 (14B)	36	48	5120	8000	1000
Qwen 2.5 (72B)	60	80	8192	12000	1000
Mistral-Small (24B)	30	40	5120	8000	1000
Gemma 2 (27B)	35	48	4608	8000	1000

C Entropy as the uncertainty estimator

Entropy is a widely used estimator for measuring uncertainty over multiple responses in prior studies [20, 29, 28]. However, entropy is not applicable to continuous values such as longitudes and latitudes in spatial datasets. In Table 4, we adopt entropy as the uncertainty estimator to measure variation in temporal responses. Figure 8 includes the trend between response uncertainty and probe performance across segments. Experimental results show that our conclusions still hold under this metric.

Table 4: Correlation between probe performance and LLM response uncertainty on Llama 3.1 (8B, 70B), Qwen 2.5 (14B, 72B), Mistral-Small (24B), and Gemma-2 (27B) across three temporal datasets.

Dataset	LLama 8B		LLama 70B		Qwen 14B		Qwen 72B		Mistral 24B		Gemma 27B	
	K	Sp	K	Sp	K	Sp	K	Sp	K	Sp	K	Sp
<i>Correlation coefficient: response uncertainty (entropy) vs probe performance (R^2).</i>												
Figures	-0.96	-0.87	-0.90	-0.77	-0.82	-0.76	-0.96	-0.85	-0.97	-0.89	-0.99	-0.95
Artworks	-0.99	-0.98	-0.99	-0.96	-0.97	-0.90	-0.87	-0.71	-0.98	-0.91	-0.88	-0.76
News	-0.99	-0.97	-0.99	-0.98	-0.94	-0.88	-0.91	-0.81	-0.96	-0.90	-0.98	-0.90
<i>Correlation coefficient: response uncertainty (entropy) vs probe performance (Spearman rank score).</i>												
Figures	-0.98	-0.99	-0.90	-0.97	-0.90	-0.83	-0.80	-0.93	-0.91	-0.97	-0.96	-0.99
Artworks	-0.97	-0.99	-0.98	-0.99	-0.88	-0.96	-0.80	-0.91	-0.91	-0.98	-0.90	-0.97
News	-0.95	-0.98	-0.98	-0.99	-0.89	-0.95	-0.81	-0.90	-0.96	-0.83	-0.93	

- 'K' and 'Sp' denote the Kendall and Spearman rank correlation coefficients respectively.

D The linearity of correlation

One interesting question is whether the correlation between response uncertainty and probe performance is linear. To investigate this, we report the Pearson correlation coefficients on three temporal datasets, as shown in Table 5. We include both variance and entropy as uncertainty estimators in our analysis. Recognizing that different uncertainty estimators operate on different scales—and that probe performance itself is unaffected by the choice of uncertainty measure—we observe that the linearity of the correlation depends on the specific uncertainty estimator used. This observation may also explain why Kossen et al. [28] could train a linear model to predict uncertainty (semantic entropy) from hidden representations.

Table 5: Pearson coefficient between probe performance and LLM response uncertainty on Llama 3.1 (8B, 70B), Qwen 2.5 (14B, 72B), Mistral-Small (24B), and Gemma-2 (27B) across three temporal datasets.

Dataset	LLama 8B	LLama 70B	Qwen 14B	Qwen 72B	Mistral 24B	Gemma 27B
<i>Pearson coefficient: variance vs probe performance (R^2).</i>						
Figures	-0.46	-0.53	-0.20	-0.37	-0.48	-0.73
Artworks	-0.36	-0.54	-0.20	-0.52	-0.50	-0.30
News	-0.07	-0.24	-0.3	-0.15	-0.54	-0.40
<i>Pearson coefficient: variance vs probe performance (Spearman rank score)</i>						
Figures	-0.40	-0.56	-0.36	-0.26	-0.61	-0.42
Artworks	-0.40	-0.57	-0.15	-0.50	-0.50	-0.25
News	-0.06	-0.32	-0.30	-0.26	-0.61	-0.42
<i>Pearson coefficient: entropy vs probe performance (R^2).</i>						
Figures	-0.93	-0.96	-0.97	-0.96	-0.95	-0.96
Artworks	-0.98	-0.98	-0.98	-0.89	-0.94	-0.91
News	-0.99	-0.99	-0.99	-0.93	-0.97	-0.94
<i>Pearson coefficient: entropy vs probe performance (Spearman rank score)</i>						
Figures	-0.96	-0.97	-0.81	-0.93	-0.97	-0.97
Artworks	-0.98	-0.99	-0.97	-0.89	-0.93	-0.96
News	-0.99	-0.99	-0.99	-0.95	-0.97	-0.92

E Additional sensitivity experiments

In this section, we present additional experimental results related to generation temperature (Figure 9), the sliding window strategy (Figure 10), and prompt templates 6 used for the probe model. Our conclusions hold across general settings, except in extreme cases—such as very high or low temperatures, overly small window sizes or large strides, or the use of complex prompts.

Table 6: The role of prompt template in correlation coefficient analysis on Llama 3.1 (8B) using the Figures dataset. ‘K’ and ‘Sp’ denotes Kendall and Spearman rank correlation coefficients, respectively.

Prompt	Variance vs R^2		Variance vs Sp	
	K	Sp	K	Sp
System prompt: Play as a historian and return the death year of given person. User prompt: when did {} die?	-0.85	-0.96	-0.49	-0.66
System prompt: Return the death year of given person. User prompt: when did {} die?	-0.75	-0.85	-0.43	-0.66
Return the death year of {}:	-0.89	-0.98	-0.67	-0.82
What is the death year of {}? only return the year.	-0.61	-0.78	-0.62	-0.76

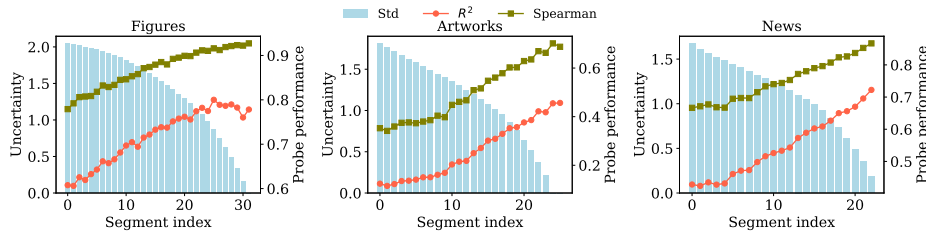


Figure 8: Trend between response uncertainty (entropy) and probe performance on the Llama 3.1 (8B) model over three temporal datasets.

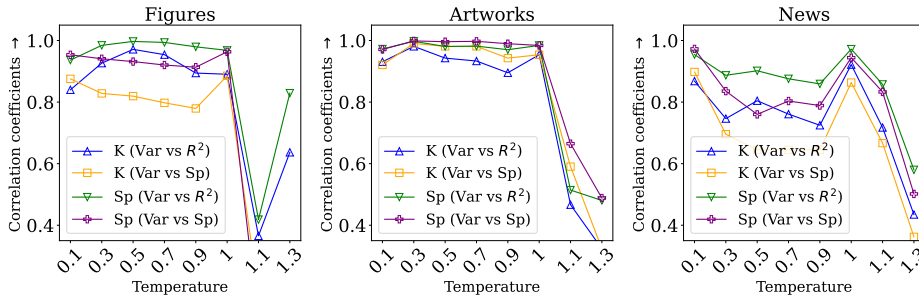


Figure 9: The correlation analysis with different temperatures in generation for Mistral-Small (24B). ‘Var’, ‘K’, and ‘Sp’ denotes variance (uncertainty estimator), Kendall and Spearman rank correlation coefficients. Here we use absolute coefficient value for good visualization performance.

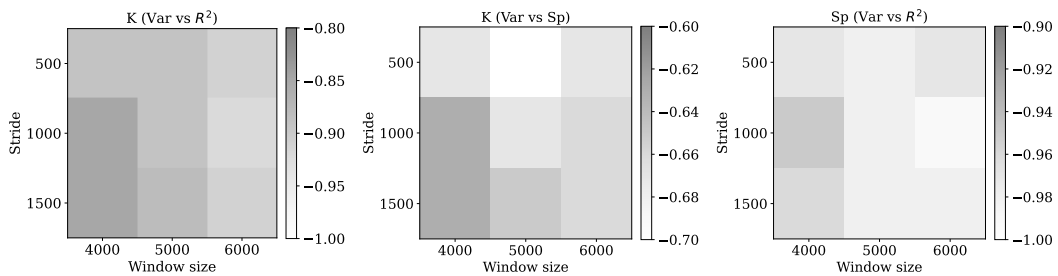


Figure 10: Correlation coefficient vs sliding window parameters, Llama 3.1 (8B) on Figures. ‘Var’, ‘K’, and ‘Sp’ denotes variance (uncertainty estimator), Kendall and Spearman rank correlation coefficients.

F Additional experiments of Section 5

In this section, we present additional experiments related to Section 5. Since AttnLRP is specifically designed for the smaller Llama models, and does not support Llama 3.1 (70B), we use Llama 2 (14B) to study whether the probe model and the generation process rely on similar features in the input representation $\phi(x)$. The experimental results are shown in Figure 11. In the remove-and-retrain experiments, retaining the top 20% of important features is sufficient to achieve a good fit for the probe models.

Figure 12 reports the remove and test results on different uncertainty subsets using Artworks dataset. From the bottom figure, we can see that preserving the top 5% of important features approximately achieves the similar Spearman rank correlation for low-uncertainty subset while 30% is needed for high-certainty subset. This experiment provides additional evidence to support our hypothesis. The same conclusion holds when using entropy as the uncertainty estimator to select three subsets with varying levels of uncertainty, as shown in Figure 13.

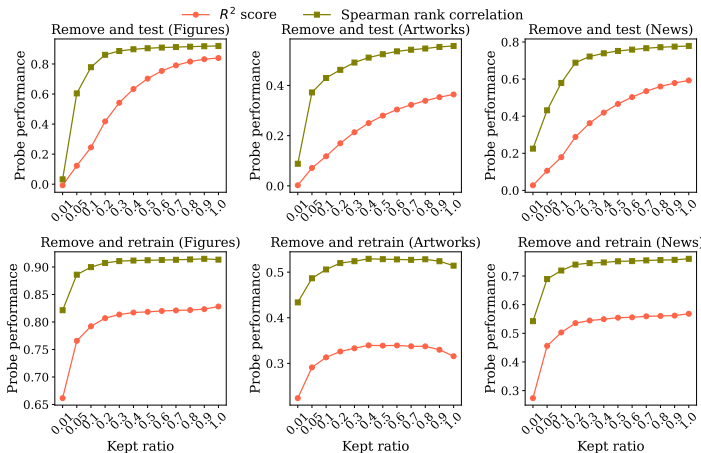


Figure 11: Llama 2 (13B) model. We gradually remove unimportant features to LLM responses and observe the probe performance drop.

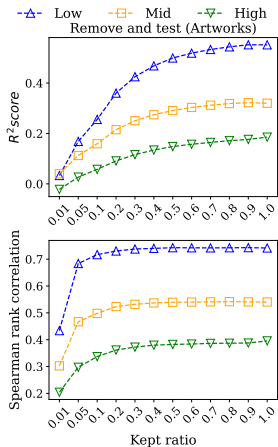


Figure 12: Remove and test on differently uncertain subsets, Llama 3.1 (8B).

G Formal analysis of section 5.2

Let us revisit the objective of investigating the underlying reasoning behind the negative correlation between response uncertainty and probe performance. Given an sample x , we obtain the embedding of the target layer l , denoted as $\phi(x)$ where the layer index is omitted for simplicity. The final response is generated by forwarding $\phi(x)$ through the remaining layers, represented by $\varphi(\phi(x))$. Due to the stochastic nature of sampling during generation, the LLM may produce different responses for the same question x , denoted by $\{r_i, \dots, r_m\}$. With the help of AttnLRP [3], we compute feature importance scores $\sigma_i(x)$ with respect to a single response r_i , where a higher value indicates that the absence of the corresponding feature would significantly affect the final output.

Recent studies [31, 45] have shown that only a small subset of features is highly important for model predictions. Consistently, our experiments demonstrate that preserving the top 20% of features yields competitive probing performance in Figure 5. Let $\hat{\phi}_i(x) \in \mathbb{R}^k \subseteq \sigma(x)$ denote the core set of important features in $\phi(x)$ with respect to response r_i , where $k \ll d$. If the model produces varying responses, the corresponding set $\hat{\phi}_i(x)$ are likely to differ, suggesting that a large number of features in $\phi(x)$ contribute to the final prediction. For example, if an LLM produces two different responses for the death year of George Washington—e.g., 1799 and 1796—different features in $\phi(x)$ will contribute to the final token position of these responses.

Next we dive into the lower probe performance of high uncertainty response from Lasso oracle inequality in compressed sensing domain [11]. For a linear regression model with an s -sparse true

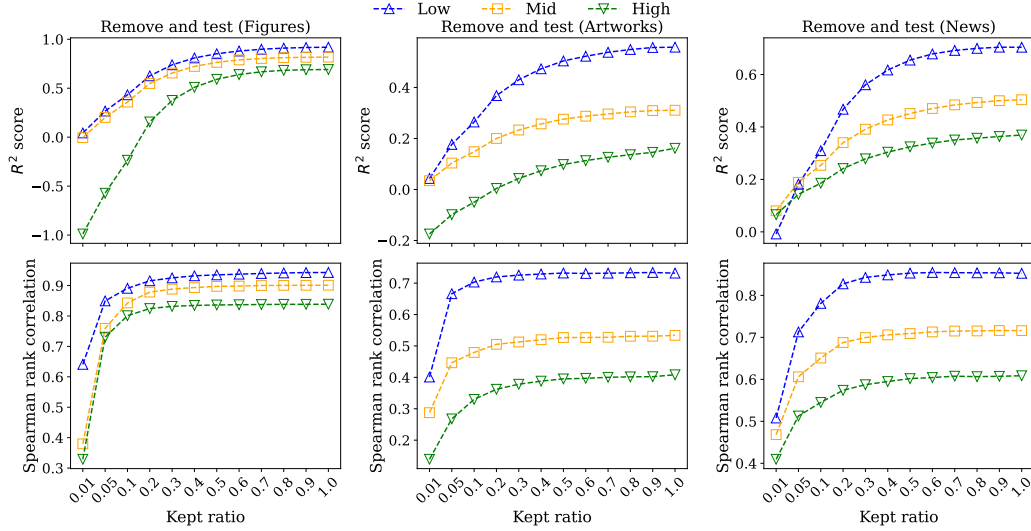


Figure 13: Remove and test on three subsets of varying uncertainty (measured by entropy), on Llama 3.1 (8B). Probe training on high-uncertainty datasets requires more features to achieve higher results.

Table 7: Prompts and response uncertainty for examples in Section 5.3.

Prompt	Entropy (Llama 3.1 (8B))
What is the category of {brand}? Only select one from [Luxury, Fashion, Sports, Casual]	0.12
What hour is after {hour}?	0

parameters, we have

$$\Pr\left[L(\hat{w}) - \widehat{L}(\hat{w}) \leq C \sigma^2 \sqrt{\frac{s \log d}{n}}\right] \geq 1 - \delta. \quad (3)$$

where,

- $L(\hat{w})$: Population (true) risk.
- $\widehat{L}(\hat{w})$: Empirical risk on n samples.
- d : Total number of available features.
- $s \ll d$: Number of *truly useful* (non-zero) features (sparsity).
- σ^2 : Noise variance / loss Lipschitz constant.
- C : Universal numerical constant.
- δ : Confidence level of the high-probability bound.

With probability at least $1 - \delta$, the gap between the empirical risk and the population (true) risk is upper-bounded by a sparsity-controlled term. For an LLM with higher response uncertainty, a larger number of features contribute to the diverse responses compared to a model with lower uncertainty, making it more difficult to achieve accurate predictions with a linear regression probe.

H Prompts in Section 5.3

We list the prompts used to query the LLM for two examples from Section 5.3 in Table 7. In both cases, the LLM produced identical responses, exhibiting very low uncertainty.